Plasma dynamics in a hollow cathode triggered discharge with the influence of fast electrons on ionization phenomena and EUV emission

2008 Plasma Sources Sci. Technol. 17 024017

(http://iopscience.iop.org/0963-0252/17/2/024017)

Plasma Sources Sci. Technol. **17** (2008) 024017 (13pp) doi:10.1088/0963-0252/17/2/024017

Plasma dynamics in a hollow cathode triggered discharge with the influence of fast electrons on ionization phenomena and EUV emission

S V Zakharov[1,4], V S Zakharov[2], V G Novikov[2], M Mond[3] and P Choi[1]

[1] EPPRA sas, 16 av. du Québec, 706 SILIC, Villebon/Yvette 91140, France
[2] Keldysh Institute of Applied Mathematics RAS, Moscow, Russia
[3] Ben-Gurion University, Beer-Sheva 84105, Israel

Received 1 October 2007, in final form 17 March 2008
Published 1 May 2008
Online at stacks.iop.org/PSST/17/024017

Abstract
The 2D computational code Z^* is used to simulate physical phenomena in a hollow cathode triggered low-pressure capillary discharge at different phases of the process: electron beam generation, formation of a channel by an ionization wave and discharge dynamics together with ionization kinetics and plasma emission, particularly in the EUV band, which is interesting for applications. Runaway electrons in a gas-filled capillary discharge with a hollow cathode play an important role both in ionization wave propagation and in ionization of multicharged ions in a discharge plasma. The electron beam prepares a tight ionized channel. The fast electrons shift the ionization equilibrium in the discharge plasma, increasing the EUV emission from the relatively low-temperature plasma of argon or xenon. At the ionization wave stage, the electron flow is simulated in an electron-hydrodynamic model. At the discharge stage, the plasma is described by the radiative magnetohydrodynamics with ionization kinetics and radiation transfer. The universal method for calculation of cross-sections of electron–ion inelastic impact processes in a plasma of multicharged ions in a wide range of plasma parameters is realized in computational code on the basis of the Hartree–Fock–Slater quantum-statistical model of a self-consistent field for the average atom and the distorted wave approximation.

1. Introduction

Discharge-produced plasmas (DPP), like the hollow cathode triggered Z-pinch, capillary discharge, laser induced pseudo-spark and laser-produced plasma (LPP), are considered as possible candidates for the creation of a compact high power EUV radiation source in 2% bandwidth around 13.5 nm spectral wavelength for the next generation of lithography applications [1]. In plasma discharges, low Z materials like Li ($Z = 3$) or various high Z materials such as Sn ($Z = 50$), In ($Z = 49$) or gases Kr ($Z = 36$), Xe ($Z = 54$), for instance, are considered for generation of EUV radiation. Transitions 5p–4f in the xenon ion Xe XI and resonances 4d–4f of a set of tin ions Sn V-XIV emit intensely in the 13.5 nm 2% bandwidth spectral band [2]. To achieve a suitable ionization degree to emit photons with 92 eV energy the high Z plasma should be heated up to tens of electron volts.

To produce the radiation in a narrow spectral band effectively the plasma should be almost transparent as the EUV range occupies only a small part of the spectrum. One of the main characteristics of plasma emitting intensely in a relatively narrow EUV band is the presence of high-intensity non-equilibrium radiation in a wide spectral range. Also, fast electrons are often present in DPP or LPP and affect the ionization degree. Therefore, most experimental plasmas of EUV sources under conditions of interest exist in the non-local thermodynamic equilibrium (non-LTE) regime. Knowledge of the behaviour of non-equilibrium plasma containing multiply charged ions (hereafter 'multicharged ion plasma') is critical for the study of DPP or LPP EUV source. Accurate numerical modelling of transient plasmas together with ionization phenomena and radiation transfer with at least

[4] Also at: RRC Kurchatov Institute, Moscow, Russia.

2D effects has been recognized as an essential part of the continuing development of plasma radiation sources.

Z^* is a 2D computational code [3] designed at EPPRA, in collaboration with the RRC Kurchatov Institute, Keldysh Institute of Applied Mathematics RAS and Troitsk Institute of Innovation and Fusion Research (TRINITI), to focus specifically on the modelling of a multicharged ion plasma in experimental and industrial facilities. It uses either a radiative magnetohydrodynamic (RMHD) approach to simulate the dynamics of quasi-neutral plasma or an electron-hydrodynamic approach to simulate flows of fast electrons in a weakly ionized gas. The code Z^* is a further development from the well-proven code ZETA [4, 5]. EPPRA is currently developing a system tool based on the adaptation of the RMHD code Z^*, to facilitate numerical modelling by non-numerical specialists. This tool, called a Z^* Black-box Modelling Engine (Z^*BME) [6, 7], is integrated into a specific computation environment to provide a turn-key simulation instrument, which does not require knowledge of numerical computation. It has been adapted, in particular, to simulate DPP and LPP radiation sources.

2. Computation code Z^*

The RMHD code Z^* for self-consistent modelling of plasma dynamics together with plasma radiation is designed on the basis of the magnetohydrodynamic (MHD) formalism of multicharged ion plasma in a 2D axially symmetric geometry with radiation transport.

2.1. RMHD of multicharged ion plasma

The traditional ideal MHD model has been extended to take into account additional physics relevant to an EUV plasma source with realistic boundaries. It is necessary to account for the displacement current in the Maxwell equation to model the situation, when the conductivity tensor turns to zero, for instance, in non-ionized neutral gas or insulator. A suitable physical model of the plasma includes a quasi-neutral plasma MHD description in a self-consistent electromagnetic field with ionization and radiation. In the MHD model a 'zero mass' electron motion (generalized Ohm's law) with effective conductivity is considered as well as the energy exchange between the 'electron' plasma component and the 'heavy' (i.e. ions and neutrals) component, the thermal conduction and the radiation. The system of equations for the plasma mass density ρ, average plasma velocity $\vec{v}$, two temperatures $T_{e,i}$ in the self-consistent electro magnetic field $\vec{E}$, $\vec{B}$ in the RMHD approximation is (Gaussian units are used)

$$
\begin{aligned}
&\frac{\partial \rho}{\partial t} + \nabla(\rho \vec{v}) = 0;\\
&\rho\left(\frac{\partial \vec{v}}{\partial t} + (\vec{v}\nabla)\vec{v}\right) = -\nabla p + \frac{1}{c}\vec{j}\times\vec{B} - \nabla\hat{\pi}_{ii}; \quad p = p_e + p_i\\
&\nabla\times\vec{E} = -\frac{1}{c}\frac{\partial \vec{B}}{\partial t}; \quad \nabla\times\vec{H} = \frac{4\pi}{c}\vec{j} + \frac{1}{c}\frac{\partial \varepsilon\vec{E}}{\partial t};\\
&\nabla\vec{B} = 0; \vec{B} = \qquad \mu\vec{H}\\
&\vec{j} - \hat{\sigma}\frac{\vec{u}\times\vec{B}}{c} = \hat{\sigma}\left(\vec{E}^* + \frac{\nabla p_e}{en_e}\right); \quad \vec{E}^* = \vec{E} + \frac{1}{c}\vec{v}\times\vec{B};\\
&\vec{u} = -\frac{\vec{j}}{en_e}\\
&\rho\left(\frac{\partial \varepsilon_e}{\partial t} + ((\vec{v}+\vec{u})\nabla)\varepsilon_e\right) = -p_e\nabla(\vec{v}+\vec{u}) - \nabla\vec{W}_e + \vec{j}\hat{\sigma}^{-1}\vec{j}\\
&\quad + Q_{ei} - \nabla\vec{F}_r + G\\
&\rho\left(\frac{\partial \varepsilon_i}{\partial t} + (\vec{v}\nabla)\varepsilon_i\right) = -p_i\nabla\vec{v} - \nabla\vec{W}_i - Q_{ei} - \hat{\pi}_{ii}\nabla\vec{v};\\
&\quad W_{e,i} = -\hat{\kappa}_{e,i}\nabla T_{e,i}.
\end{aligned}
\tag{1}
$$

The radiation flux density F_r in the electron energy equation is calculated by means of the radiation transport equation considered below. The term G is introduced to take into account possible external heating, by laser light for example. The laser interaction with the substance needs to be considered separately [3] and is not discussed here.

The quasi-neutral plasma means $n_e \approx \bar{Z}n_i = \bar{Z}\frac{\rho}{m_i}$, as $\bar{Z}m_e/m_i \ll 1$. The Poisson equation is not introduced separately to avoid introducing a new value such as the charge density. It is fulfilled automatically from the second Maxwell equation due to the fact that $\nabla(\nabla\times\vec{H}) = 0$, if initial conditions for the electric field satisfy the Poisson equation. In view of the special practical application of the physical equations we assume that at the initial time moment $\nabla\varepsilon\vec{E}\big|_{t=0} = 0$ everywhere in the space except at, perhaps, the conductor boundaries. The dielectric constant ε and magnetic permeability μ are introduced to describe homogeneously the plasma dynamics together with the electromagnetic field behaviour in insulators and metallic objects (if necessary). For the plasma and gas $\varepsilon = \mu = 1$ are imposed. Different plasmas and solid materials may be considered as differing from each other only by their properties, especially if solid materials can be sublimated and transformed to the plasma medium. These properties of plasmas and other substances are described by the equation of state (EOS), i.e. thermal pressure $p_{e,i}(\rho, T_{e,i}, \bar{Z})$, specific internal energy $\varepsilon_{e,i}(\rho, T_{e,i}, \bar{Z})$ and ionization degree $\bar{Z}(\rho, T_{e,i}, U, t)$; by kinetic coefficients and tensors, i.e. electron–ion energy exchange rate $Q_{ei}(\rho, T_{e,i}, \bar{Z})$, by conductivity $\hat{\sigma}(\rho, T_e, \bar{Z}, \vec{B}, \vec{u})$, thermal conductivities $\hat{\kappa}_{e,i}(\rho, T_e, \bar{Z}, \vec{B}, \vec{u})$, ion viscosity $\hat{\pi}_{ii}(\rho, T_e, \bar{Z}, \vec{B}, \vec{v})$ and radiation properties mentioned above. The dependence of coefficients on the magnetic field are described in [8].

It is necessary to outline that, due to non-stationary effects, the ionization degree $\bar{Z}$ depends not only on the plasma density and temperature but also on time, through the ionization kinetics described by level kinetic equation (2). The dependence of the conductivities on the electron drift velocity $\vec{u}$ is described through the concept of the anomalous resistivity in the low-density plasma regions due to plasma turbulence: the low-hybrid drift and ion sound waves as having low thresholds. The EOS and the kinetic coefficients are obtained by means of the cross-sections of collisional processes between the electrons, ions and atoms and the interaction with radiation calculated in the framework of the general quantum-statistical model and ionization kinetics described below. Plasma radiation properties, ionization and the EOS, as well as

excitation and ionization rates and plasma kinetic coefficients, are calculated by means of interpolations from a set of tables prepared in pre-processing with the Hartree-Fock-Slater (HFS) model [9] in both the optically thick LTE, and the transparent non-LTE limits. The actual non-LTE condition at any instant is modelled by analytical interpolation between these two limits [5]. Another set of tables prepared by the pre-processor is used for the post-processing treatment of data obtained by the RMHD processor, to calculate detailed spectra of the plasma emission with high resolution in specific spectral bands, such as EUV or other regions as desired. Interpolations of preliminary prepared databases allow the code to avoid on-line calculations of absolutely different processes like the plasma dynamics, the atomic physics and ion kinetics. As a result, the robustness of the code and the accuracy of the calculations of the main processes are enhanced considerably.

2.2. *Radiative and ionization properties of a plasma*

To accurately investigate the physical processes in a complex plasma, information about properties of matter in a wide range of plasma parameters, including rate coefficients of radiative, collisional ionization and recombination (plus dielectronic one) for multicharged ions, is required. These values may be obtained by using a proper atomic model. Furthermore, in practical plasmas, the complete level kinetics consideration should be applied to describe the ionization processes and emission spectra. Calculation of the emission spectra from a small-size plasma of high current pulsed systems and LPPs requires taking into consideration reabsorption of the radiation by the plasma, in the presence of high-intensity non-equilibrium radiation. In a comparatively simple case the problem may be considered by using the Biberman–Holstein approximation, which is valid in cases when spectral lines do not overlap. This is not applicable for a multicharged ion plasma, where there are a lot of overlapping spectral lines. On the other hand, the full system of the level-population kinetics equations including the processes induced by non-equilibrium radiation field is complicated for direct calculations. In addition, in a detailed approach, it is difficult to describe correctly all important states and transitions with all necessary processes in multicharged plasmas such as plasmas of xenon or tin at the tenth degree of ionization. However, these factors alone do not limit the wide application of the full level kinetics.

For practical applications, the numerical procedure should be comparatively simple and its cost, in terms of computation time, must be low enough to be used in 2D RMHD simulations. One suitable solution is to use an average atom model [10] where all possible states and transitions are accounted for. In this approximation an average ion with mean occupation numbers N_ν in the state $\nu = nlj$ (where n is the principal quantum number, l is the orbital angular quantum number and j is the quantum number of total angular momentum of the electron) is placed together with free electrons in a neutral spherical cell [9]. The non-stationary kinetics balance for average occupation numbers N_ν is given by equations [11]:

$$\frac{\mathrm{d}N_\nu}{\mathrm{d}t} = \left(1 - \frac{N_\nu}{g_\nu}\right) S_\nu - N_\nu L_\nu, \tag{2}$$

where g_ν is a statistical weight of electrons in the ν state, S_ν is the total rate of the processes leading to an increase in the number of electrons in the ν state:

$$S_\nu = \sum_{\mu<\nu} N_\mu(\alpha^{\mathrm{abs}}_{\mu\nu} + \alpha^{\mathrm{ex}}_{\mu\nu}) + \sum_{\mu>\nu} N_\mu(\alpha^{\mathrm{em}}_{\mu\nu} + \alpha^{\mathrm{dex}}_{\mu\nu}) + \bar{Z}(\alpha^{\mathrm{ir}}_\nu + \alpha^{\mathrm{phr}}_\nu + \alpha^{\mathrm{dc}}_\nu), \tag{3}$$

where $\mu = n'l'j'$, and L_ν is the total rate of processes leading to a decrease in the number of electrons in the following state:

$$L_\nu = \sum_{\mu<\nu}\left(1 - \frac{N_\mu}{g_\mu}\right)(\alpha^{\mathrm{em}}_{\nu\mu} + \alpha^{\mathrm{dex}}_{\nu\mu}) + \sum_{\mu>\nu}\left(1 - \frac{N_\mu}{g_\mu}\right) \times (\alpha^{\mathrm{abs}}_{\nu\mu} + \alpha^{\mathrm{ex}}_{\nu\mu}) + \alpha^{\mathrm{ii}}_\nu + \alpha^{\mathrm{phi}}_\nu + \alpha^{\mathrm{ai}}_\nu, \tag{4}$$

where $\alpha^{\mathrm{ex}}_{\mu\nu}$ and $\alpha^{\mathrm{dex}}_{\nu\mu}$ are rates of collisional excitation and deexcitation of level ν; α^{ii}_ν, α^{ir}_ν are rates of ionization and three-body recombination; $\alpha^{\mathrm{abs}}_{\mu\nu}$, $\alpha^{\mathrm{em}}_{\nu\mu}$ are rates of absorption and emission in spectral lines; $\alpha^{\mathrm{phi}}_\nu$, $\alpha^{\mathrm{phr}}_\nu$ are rates of photoionization and radiative recombination and α^{ai}_ν, α^{dc}_ν are the rates of Auger effect (autoionization) and dielectronic capture. The average ion charge $\bar{Z}$ determines the number of free electrons per atom, i.e. an average ionization degree is $\bar{Z} = Z - \sum N_\nu$, where Z is the nuclear charge of ions. In level kinetics calculations the rates obtained for the free ions are widely used. This is correct for low-density plasmas. With increasing density the applicability of such rates is no longer valid. As shown in [12], due to density effects the ionization and recombination rates for Xe plasma may essentially differ from those obtained for free ions.

When gas-dynamics processes proceed much slower than collisional and radiative ones, the quasi-stationary approximation can be applied. This type of quasi-stationarity is defined by rate processes, for example, as in the coronal equilibrium (CE) model [13] and the collisional–radiative equilibrium (CRE) model [10, 14, 15], which are widely used. In the quasi-stationary approximation, i.e. $\frac{\mathrm{d}N}{\mathrm{d}t} = 0$, equation (2) may be rewritten in the form:

$$N_\nu = \frac{g_\nu}{1 + g_\nu L_\nu / S_\nu}. \tag{5}$$

This equation is still nonlinear, as the rates S_ν and L_ν depend on the average occupation numbers N_ν, which for high Z elements may be solved only numerically. Solving these equations we obtain under given radiation field I_ω the elemental states of a quasi-stationary plasma: the average occupation numbers, energy levels and wave functions of electrons. From these elements, we calculate the ionization degree, EOS, spectral absorption and emission coefficients and necessary kinetic coefficients (such as thermal and electric conductivity elastic collision rate) in the plasma.

The collisional rates can be calculated in the distorted wave approximation (DWA) [16], or other well-known formulae [10, 17]. Oscillator strengths, energy levels and other values are calculated on the basis of the relativistic HFS model [9] depending on the occupancies N_ν. A universal computational method based on the DWA [16] and semi-classical wave functions of electrons calculated in the HFS

quantum-statistical model of self-consistent field [9] is applied for impact electron–ion cross-sections calculations.

Cross-sections of impact processes are calculated from the single-electron approach using the configuration-average DWA. For single-electron excitation in the ion from the state γ_0 to the state γ (with electron excitation $(n\ell \to n'\ell')$ [18]:

$$\sigma^{\mathrm{ex}}_{\gamma_0\gamma} = \sum_{\kappa} \left[\sigma'_{\kappa}(n\ell, n'\ell') + \sigma''_{\kappa}(n\ell, n'\ell')\right]. \tag{6}$$

Here $\sigma'_{\kappa}(n\ell, n'\ell')$ includes direct and interference parts, $\sigma''_{\kappa}(n\ell, n'\ell')$ is the exchange part:

$$\sigma'_{\kappa}(n\ell, n'\ell') = \frac{4\pi^3}{k^2} \sum_{\lambda,\lambda'} P^d_{\kappa} \left(P^d_{\kappa} - \sum_{\kappa'} P^e_{\kappa',\kappa} \right),$$

$$\sigma''_{\kappa}(n\ell, n'\ell') = \frac{4\pi^3}{k^2} \sum_{\lambda,\lambda'} \left(\sum_{\kappa'} P^e_{\kappa'\kappa} \right)^2. \tag{7}$$

Here λ, λ' and ε, ε' are quantum moments and energies of incident electron before and after collision, $k = (2\varepsilon)^{1/2}$. Direct P^d_{κ} and $P^e_{\kappa'\kappa}$ exchange radial integrals may be introduced through $3jm$ and $6j$ Wigner coefficients as follows:

$$P^d_{\kappa} = \sqrt{\frac{(2\ell'+1)(2\lambda+1)(2\lambda'+1)}{2\kappa+1}} \times \begin{pmatrix} \kappa & \ell & \ell' \\ 0 & 0 & 0 \end{pmatrix} \begin{pmatrix} \kappa & \lambda & \lambda' \\ 0 & 0 & 0 \end{pmatrix} R^{(\kappa)}_{n\ell,n'\ell';\varepsilon\lambda,\varepsilon'\lambda'},$$

$$P^e_{\kappa'\kappa} = (-1)^{\kappa+\kappa'} \sqrt{(2\kappa+1)(2\ell'+1)(2\lambda+1)(2\lambda'+1)} \times \begin{pmatrix} \kappa' & \ell & \lambda' \\ 0 & 0 & 0 \end{pmatrix} \begin{pmatrix} \kappa' & \lambda & \ell' \\ 0 & 0 & 0 \end{pmatrix} \begin{Bmatrix} \kappa' & \ell & \lambda' \\ \kappa & \lambda & \ell' \end{Bmatrix} R^{(\kappa')}_{\varepsilon\lambda,n'\ell';n\ell,\varepsilon'\lambda'}. \tag{8}$$

Slater's integrals

$$R_{\alpha,\beta;\gamma,\delta(\kappa)} = \iint R_{\alpha}(r') R_{\beta}(r') \frac{r^{\kappa}_{<}}{r^{\kappa+1}_{>}} R_{\gamma}(r'') R_{\delta}(r'')\, \mathrm{d}r'\, \mathrm{d}r'' \tag{9}$$

include radial parts of single-electron wave functions of discrete and continuous spectra. Radial parts of the ion electron's wave functions are calculated in the self-consistent HFS potential by numerical solution of Schrödinger's equation and radial parts of the free electron's wave functions are calculated in the HFS potential by improved semi-classical approximation on the base of Bessel's functions [9].

For the calculation of impact ionization differential cross-section of the ion from the state γ_0 to the state γ (by ejecting an electron from shell $n\ell$ to the continuum state with energy ε^* and orbital momentum λ^*) in excitation cross-section formulae, it is necessary to change the final state of electron of discrete spectra $n'\ell'$ to the continuum spectra $\varepsilon^*\lambda^*$:

$$\mathrm{d}\sigma_{\gamma_0\gamma} = \sum_{\kappa} \left[\sigma'_{\kappa}(n\ell, \varepsilon^*\lambda^*) + \sigma''_{\kappa}(n\ell, \varepsilon^*\lambda^*)\right] \mathrm{d}\varepsilon^*. \tag{10}$$

The ionization cross-section is

$$\sigma^{ii}_{\gamma_0\gamma} = \sum_{\lambda^*} \int_0^{(\varepsilon-\varepsilon^i)/2} \frac{\mathrm{d}\sigma_{\gamma_0\gamma}}{\mathrm{d}\varepsilon^*}\, \mathrm{d}\varepsilon^*, \tag{11}$$

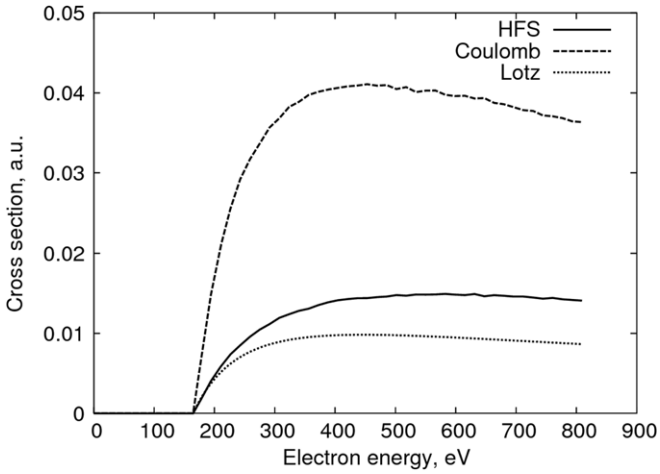

Figure 1. Single-electron ionization cross-sections of 4d shell for Xe^{8+} calculated in the DWA using the HFS potential and the Coulomb potential in comparison with the Lotz formula [17].

where ε^i is the energy of ionization. In general orbital momenta λ, λ', λ^* of free electrons are limited by the value $\lambda_{\max}$ that may be found from the existence condition of domain of classical motion of the electron with the energy ε in potential $V(r)$ on the boundary of the spherical cell with radius r_0, given by the inequality

$$2\varepsilon + 2V(r_0) - \frac{\lambda_{\max}(\lambda_{\max}+1/2)}{r_0^2} > 0. \tag{12}$$

The range of the values κ and κ' is similar:

$$\kappa_{\min} \leqslant \kappa \leqslant \kappa_{\max}, \quad \kappa'_{\min} \leqslant \kappa' \leqslant \kappa'_{\max},$$

$$\kappa_{\min} = \max(|\ell' - \ell|, |\lambda' - \lambda|), \quad \kappa_{\max} = \min(\ell + \ell', \lambda + \lambda'),$$

(for the ionization ℓ' is replaced by λ^*)

$$\kappa'_{\min} = \max(|\ell' - \lambda|, |\lambda' - \ell|), \quad \kappa'_{\max} = \min(\ell' + \lambda, \lambda' + \ell).$$

The potential field used in the calculations of wave functions of free electrons has a profound effect on the value of the cross-section (figure 1). Results of computations with the HFS potential significantly differ from calculations in the Coulomb-like potential usually used. The HFS potential, like a real potential, depends on plasma density; consequently cross-section also depends on plasma density. In figure 2, for the excitation in Xe^{10+}, it is shown that such influence may achieve 80% of the value.

The rate of impact process $\alpha_{\gamma_0\gamma}$ is determined by cross-section $\sigma_{\gamma_0\gamma}$ and the electron's distribution function by the energies $F(\varepsilon)$:

$$\alpha_{\gamma_0\gamma} = N_e a_0^3 \nu_0 \langle \sigma_{\gamma\gamma_0} v \rangle = N_e a_0^3 \nu_0 \int_{\varepsilon_t}^{\infty} \sqrt{2\varepsilon}\, \sigma_{\gamma_0\gamma}(\varepsilon) F(\varepsilon)\, \mathrm{d}\varepsilon, \tag{13}$$

where ε^t is the transition energy in the case of excitation and $\varepsilon^t = \varepsilon^i$ in the case of ionization, N_e is the electron density. Examples of collisional rates calculated in the DWA for ionization of Xe X to Xe XI ion and excitation rates of the 4d–5p transition of Xe XI are presented in figure 3 [12].

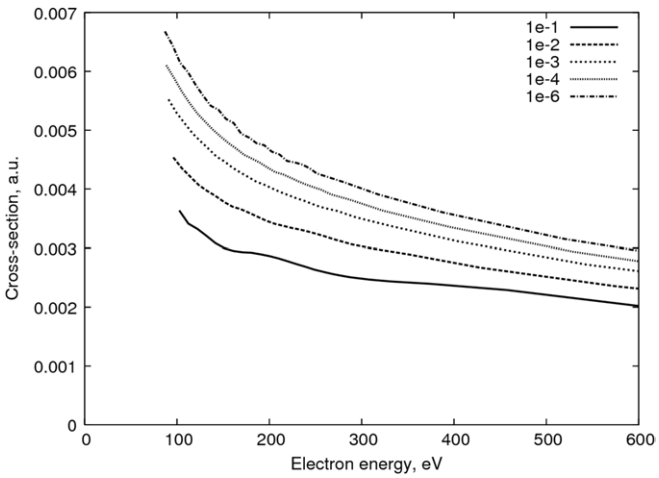

Figure 2. Single-electron impact excitation 4d–5p cross-sections for Xe^{10+} in plasma at different densities (from 10^{-6} to 10^{-1} g cm^{-3}).

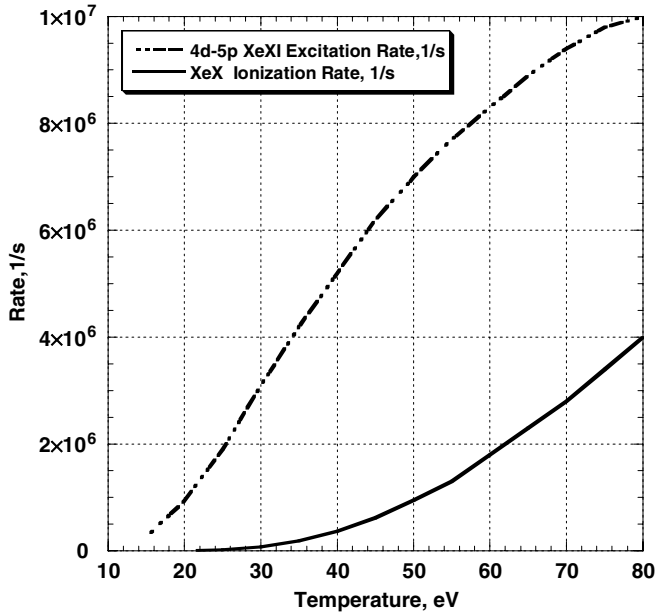

Figure 3. Ionization rate of the Xe X ion (solid line) and excitation rate of 4d–5p transition of the Xe XI ion (dashed line) versus temperature for plasma ion density 4.6×10^{15} cm^{-3}.

2.3. Radiation transfer

The photo-process rates are calculated in terms of the corresponding cross-sections taking into account the radiation field [19]. The relevant formulae may be found in [11]. As the rates and mean charge depend on the occupancies N_ν, equations (2)–(4), even in the average ion model, are non-linear and depend on the radiation field.

The influence of non-equilibrium radiation on the properties of a plasma is demonstrated on the xenon emission spectra in figure 4, where the emissivity of xenon is calculated at a temperature $T_e = 30$ eV and density $\rho = 10^{-6}$ g cm^{-3}. The calculations were carried out without and with taking into account the radiation field, assuming that up to 0.4% of radiation is reabsorbed. It is apparent from the figures that back influence of radiation on the spectral characteristics of the plasma and ionization degree is important. Partial radiation trapping can induce a significant deviation from the optically thin CE or CRE approximations for non-LTE plasma description as well as from LTE. Meanwhile, at high temperatures the radiation field is formed in the process of plasma dynamics, affecting the microstates of the plasma ions, and the radiative properties of the plasma. Respectively, the microstates of the ions determine the emissivity and spectral absorption coefficients of the plasma. Reabsorption in the spectral lines can change the ionization stage and internal energy of the plasma at the same electron temperature, as these are strongly coupled to the electrons via level kinetics.

The radiation transfer equation for spectral intensity I_ω with photon energy $\hbar\omega$, without free electron scattering processes, has the form

$$\frac{1}{c}\frac{\partial I_\omega}{\partial t} + (\vec{\Omega}\nabla)I_\omega = j_\omega - k_\omega I_\omega, \tag{14}$$

where c is the speed of light, $\vec{\Omega}$ is the unit vector in the direction of the radiation ray. The spectral absorption coefficient k_ω and emissivity j_ω are written in a form taking into account an induced emission. They depend on the local properties of a plasma, e.g. density and temperature and the ion distribution, which, in turn, are dependent on the radiation field and should be calculated in non-LTE, i.e. depending on the spectral radiation field through the level occupancy balance considered in the previous section. From the radiation transport equation (14) the radiation energy density $U = c^{-1}\int\int I_\omega \,\mathrm{d}\vec{\Omega}\,\mathrm{d}\omega$ and flux $\vec{F}_r = \int \vec{F}_\omega \,\mathrm{d}\omega = \int \vec{\Omega} I_\omega \,\mathrm{d}\omega\,\mathrm{d}\vec{\Omega}$ are calculated and used in the energy balance of the RMHD system of equations (1).

As a rule the characteristic size of the DPP or LPP plasma of interest is much smaller than the distance traversed by the radiation during the evolution time, and the quasi-stationary approximation may be applied, i.e. the time derivative in equation (14) may be neglected. To find the radiation field in the quasi-stationary case, by integrating the radiation transport equation (14) along the trajectories under cylindrical symmetry conditions, we obtain an expression for the intensity [11]:

$$I_\omega(r, z, \varphi, \theta) = \int_0^\tau \frac{j_\omega}{\kappa_\omega} e^{\tau'-\tau}\,\mathrm{d}\tau, \tag{15}$$

where r, z are the radial and axial coordinates; φ, θ are the spherical angle coordinates of the trajectory: φ between the trajectory projection onto a plane perpendicular to the Z-axis and the radial direction, and θ between the trajectory and the Z-axis; $\tau = \tau(x) = \int_0^x \frac{\kappa_\omega(r,z)}{\sin\theta}\,\mathrm{d}x$ is the optical depth, $\tau' = \tau(x')$. The coordinate $x = x(r, \varphi)$ is taken along the projection of the ray onto a plane perpendicular to the Z-axis. It is related to the radius r and angle φ of the direction of this projection by $x = \sqrt{r_{\mathrm{out}}^2 - r^2\sin^2\varphi} + r\cos\varphi$, where r_{out} is some external radius where boundary conditions on radiation may be defined as only outcoming radiation exists at $r = r_{\mathrm{out}}$, i.e. $I_\omega\big|_{r=r_{\mathrm{out}}} = 0$ at $\pi/2 < \varphi < 3\pi/2$. The coordinate z of a trajectory is defined by the formula $z = z_{\mathrm{out}} + x \cdot \mathrm{ctg}\,\theta$, where z_{out} is a coordinate of a cross point of the trajectory and the $r = r_{\mathrm{out}}$ surface.

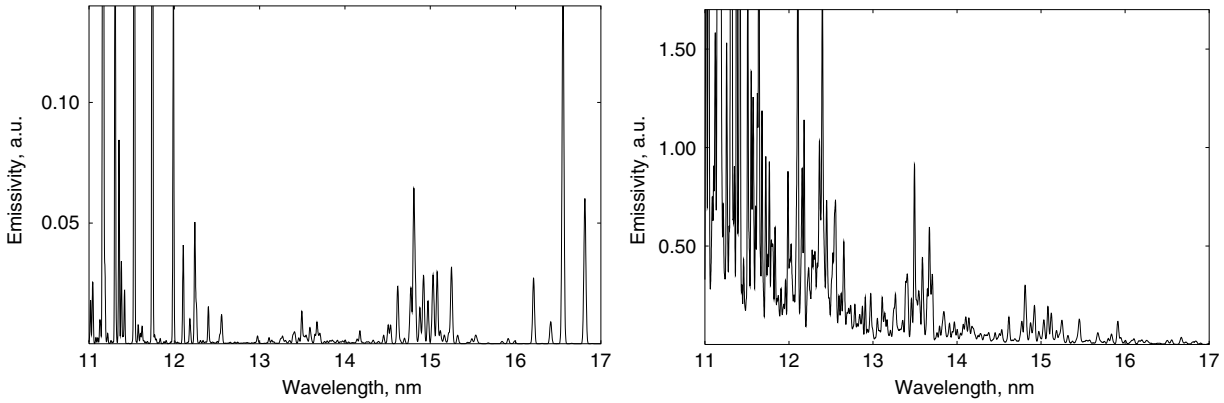

Figure 4. Emission spectra of xenon plasma versus wavelength λ at temperature 30 eV without reabsorption (left) ($\bar{Z} = 8.31$) and with ∼ 0.4% of radiation reabsorbed (right) ($\bar{Z} = 10.74$). Additional broadening is 0.05 eV.

2.4. Non-stationary and non-equilibrium plasma effects

In fast discharges the plasma is usually at quite a low density. As we can see from the calculated ionization and excitation rates in figure 3, the stationary condition will not be reached during the discharge time. In this case the steady-state solution (5) can only be used for estimations. Alternatively, special tables can be constructed and interpolated for non-stationary processes. The databases are calculated in steady-state approximations. To be able to take into account non-stationary effects in the plasma state, the rates of atomic processes calculated in the DWA [3, 20] are used by means of the simplified equation

$$\frac{\mathrm{d}f}{\mathrm{d}t} = S \cdot (\Phi(f) - \Phi(f_{\mathrm{eq}})) \tag{16}$$

applied for the mean charge, radiation coefficients and other atomic parameters f being used in the RMHD equations. The effective rate $S(T_e, \rho, \bar{Z})$and the corresponding steady-state value f_{eq} are recalculated and interpolated by means of a corresponding interpolating function $\Phi(f)$ (normalized to unity by the maximum value $\Phi_{\max}(f) = 1$) from tables prepared in pre-processing.

The influence of fast electrons on ionization degree is also taken into account [21]. Non-equilibrium distribution of electrons in the plasma, especially the presence of fast electrons, may significantly increase the ionization rate. The energy distribution of free electrons in the presence of fast electrons may essentially differ from the normal distribution (Maxwell function). Let us introduce the distribution function as the sum of normal and fast parts:

$$F(\varepsilon) = (1 - \xi) F_0(T, \varepsilon) + \xi F_0(E, \varepsilon), \tag{17}$$

where T is the electron plasma temperature, $\xi \ll 1$ is the relative portion of fast electrons, E is the average energy of fast electrons and under distribution $F_0(\theta, \varepsilon)$ we took the Maxwellian function

$$F_0(\theta, \varepsilon) = \frac{2}{\sqrt{\pi}} \sqrt{\varepsilon} \theta^{-3/2} \mathrm{e}^{-\varepsilon/\theta}. \tag{18}$$

To obtain the ionization rates with the presence of fast electrons the electron distribution function (17) should be inserted into the integral in (13). The impact recombination rate depends mainly on slow electrons; the fast electrons do not have any significant influence on it (due to its high energy and low density). In this case, it is possible to apply the detailed balance principle for the ionization rate found for the equilibrium electron distribution function. The same is true for the dielectronic and photorecombination rates, which may also be found from equilibrium formulae.

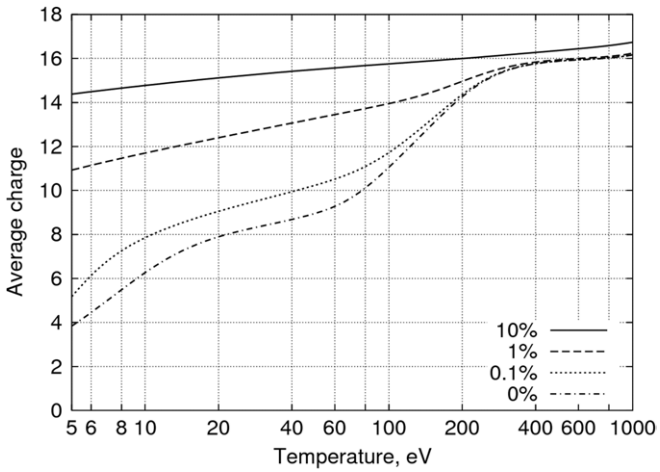

Figure 5. Ionization degree in argon plasma with fast electrons at the energy 5 keV and various percentage (0%, 0.1%, 1%, 10%).

Analysis of the influence of fast electrons on ionization equilibrium in a non-equilibrium multicharged ion plasma was made for the argon plasma in the temperature range from 5 to 1 keV with fast electrons with energies from 1 to 10 keV and relative portions of 0.1–10%. The density of free electrons in the plasma was ∼ 10^{18} cm^{-3}. The degree of influence of fast electrons with various energies and percentages is shown in figures 5 and 6. In plasmas with Maxwell electron distribution, the rate of impact ionization process is determined in general by cross-sections in a narrow range of electron energies near thresholds depending on the plasma temperature. In plasmas with fast electrons, the high energy range may also have a significant influence on the ionization rate. In such cases, it is important to use methods for the cross-section calculation applicable to a wide range of electron energies with a high enough accuracy such as the DWA.

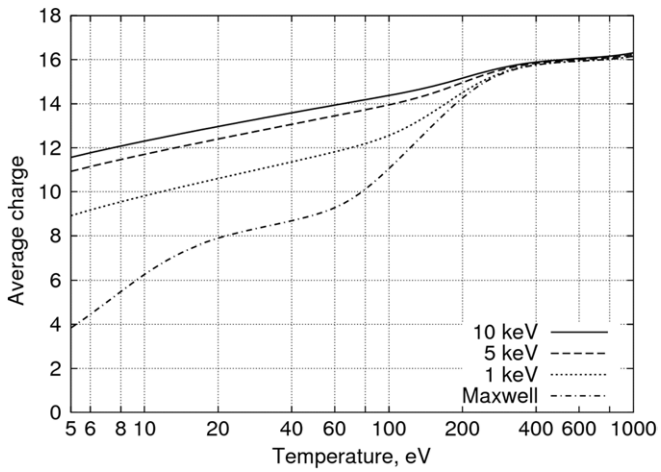

Figure 6. Ionization degree in argon plasma with fast electrons at various energies (1, 5, 10 keV) and relative portion 1% in comparison with the equilibrium distribution of electrons.

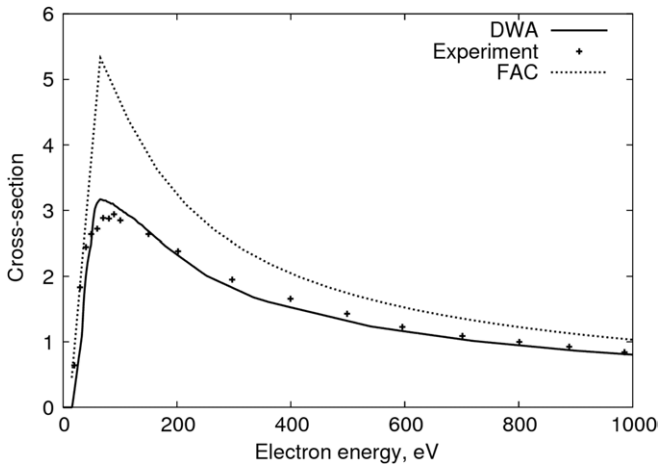

Figure 7. Ionization cross-sections (in 10^{-16} cm^2) for atomic Ar calculated in DWA in comparison with experimental data and FAC computation.

Comparison results of computation with experimental data [22] and results by flexible atomic code (FAC) [23] are presented in figure 7. The DWA demonstrates the high accuracy.

2.5. Weakly ionized plasma model

Weakly ionized plasmas may be described by equations analogous to MHD equations only if the quasi-neutrality condition is satisfied and the electron inertia is negligible, i.e. at a sufficient degree of ionization. These conditions are not fulfilled at the beginning of the ionization process, especially in the pre-ionization stage or triggering of a discharge. In general, the Boltzmann kinetic equation for electrons with ionization kinetics should be used. This general approach is not used in the code currently developed and will not be discussed in more detail here. Instead, we will consider the specific case of the hollow cathode system, which is widely used in EUV plasma sources. The hollow cathode effect [24] is considered in the electron-hydrodynamic approach. In this model, the electrons are considered flowing in a self-consistent 2D electromagnetic field [3]. The atoms and ions once ionized are supposed to be motionless.

Following [25], the electrons in a weakly ionized plasma are described by hydrodynamic equations, i.e.

$$\frac{\partial \vec{u}}{\partial t} + (\vec{u}\nabla)\vec{u} = -\frac{e}{m_e}(\vec{E} + \frac{1}{c}\vec{u} \times \vec{B}) - R_{\text{eff}} n_a \vec{u} - R_{ei} n_i \vec{u}, \tag{19}$$

where $n_a = N - n_i$ is the neutral atom density, N is the total density of 'heavy particles' (neutrals and ions), with self-consistent electromagnetic field

$$\nabla \times \vec{E} = -\frac{1}{c}\frac{\partial \vec{B}}{\partial t}; \qquad \nabla \times \vec{B} = -\frac{4\pi}{c} e n_e \vec{u} + \frac{1}{c}\frac{\partial \vec{E}}{\partial t};$$
$$\nabla \vec{E} = 4\pi e(n_i - n_e); \qquad \nabla \vec{B} = 0, \tag{20}$$

and ionization processes

$$\frac{\partial n_e}{\partial t} + \nabla(n_e \vec{u}) = n_a n_e S - n_i n_e (L_{\text{ph}} + n_e L_3),$$
$$\frac{\partial n_i}{\partial t} = n_a n_e S - n_i n_e (L_{\text{ph}} + n_e L_3). \tag{21}$$

The specific friction rates in the equation of motion (19) are defined by the inelastic and elastic collisions of electrons with atoms $R_{\text{eff}} = u(\Sigma_{\text{in}} + \Sigma_{\text{el}})$ and ions $R_{\text{ei}} = u\Sigma_{ei}$, where $\Sigma_{\text{in,el,ei}}$ are the respective cross-sections. Important features of the cross-sections for the considered phenomenon are the presence of a maximum on the ionization cross-section (for heavy elements such as Ar, it is at 80 eV) and rapid decrease of all cross-sections, at least like $\sim u^{-2}$, at higher energy (see figure 7). Specific rates S , L_{ph} and L_3 in (21) are defined by the respective cross-sections of impact ionization, photo- and 3-body recombination interpolated from a set of tables prepared in the pre-processing described above.

3. Capillary discharge EUV radiation sources

DPP EUV radiation sources belong to a class of discharge plasmas where a driving current flows along a mainly axial direction—the Z-pinch. In the Z-pinch, high density plasma is created by the driving current through electromagnetic forces [26], and heated to a high temperature by the same current. Properly designed, such a high energy density tight plasma structure efficiently transfers electrical energy into radiation. At the same time, it is known from the experience of Z-pinch plasma study that such a plasma is unstable to $m = 0$ MHD neck instability, $m = 1$ kink mode and other $m > 1$ 3D instabilities. The neck or sausage instability creates a localized region of high density and high temperature. The density and temperature are limited due to plasma outflow and hence destruction of the MHD Z-pinch structure [27]. On the other hand, in high-Z plasma, such as that encountered in the DPP EUV sources, the radiation rate is high and it is possible to utilize this necking structure to create an intense radiation point. This point of extremely high energy density can be achieved when the radiation rate is higher than the

heating rate in a plasma column undergoing compression by its own magnetic pressure, a phenomenon sometimes referred to as 'radiative collapse', or more appropriately, radiation assisted magnetic compression. The key issue for EUV source application is whether this phenomenon can be controlled and whether the electrical energy in the system can be transferred to this point-like structure, in time and in space, and can be efficiently converted to EUV radiation [28]. The neck formation may be provoked by means of, for example, initial density distribution, or by special electrode form, or by organization of special dynamics of the current sheath.

During pinch dynamics the plasma conductivity limits a rising current to flow along a certain thickness on the surface of the plasma, defined by the skin depth [30]. In a large volume discharge the current flows initially in a layer much thinner than the chamber size and forms a current sheath. The sheath is accelerated by the magnetic field pressure and compresses the plasma ahead of it. In cylindrical systems, it compresses down onto the axis, i.e. the column of plasma pinches down. As the compression rate is higher than the local sound speed, a shock wave is produced ahead of the compressing sheath structure. It ionizes and collects the gas during its motion, but some part of the gas is not captured into the motion and remains behind the sheath. This gas can trigger some additional current path, or current leakage, when the local voltage increases as a result of inductive and resistive effects during plasma pinching.

In a small volume discharge, as typical in a capillary discharge, another situation takes place. Due to the physical size of the capillary, the plasma dimension is less than the skin depth, i.e. magnetic field diffusion is high enough. There is no current sheath in this case and the discharge plasma is compressed by the magnetic field volumetrically [29]. The neck formation may be controlled by plasma density distribution.

A series of simulations using Z^* on plasma configurations like the capillary discharge [31, 32], dense plasma focus [33], Z-pinches [34], LPP [35, 36] or laser triggered DPP [7] has been performed, with a view to evaluating the functionality and suitability of such plasma systems for the purpose of plasma EUV radiation sources.

The capillary discharge is of interest due to the opportunity to develop a directed source with high intensity of EUV radiation in a beam [37] for the metrology, and also as a high volume-manufacturing (HVM) source for EUV lithography by means of multiplexing a large number of such emitters [38]. In a capillary discharge system, a high current is made to pass rapidly through a small diameter (less than the skin-depth) insulating tube. The operation of a gas-filled capillary discharge with small dimension requires the proper preparation of the initial current conduction path in order to avoid a wall initiated sliding spark discharge. By making a suitable hollow cathode structure to a capillary discharge, a self-generated on-axis electron beam is produced as a process of the transient hollow cathode effect [39]. This hollow cathode effect is used in low-density discharges working at the left-hand side of the Pachen curve to produce a tight (of the order of 100 μm) pre-ionized conducting channel on-axis, where the main current begins to develop and effective energy deposition from the power supply to the discharge realized. The hollow cathode system is widely used in EUV plasma sources.

3.1. 3D plasma compression

In most EUV capillary radiation sources developed [39,40], the operating gas is fed from one electrode and exhausted through the opposite electrode. The exhaust electrode connects the discharge system to the vacuum pumping system. Due to the almost Knudsen flow in the pressure regime of the operating discharge, a pressure gradient is established within the capillary, between the two electrodes. The higher pressure region is normally arranged at the cathode, in order to utilize the self-generated e-beam for axial pre-ionization [39]. It will be shown below that this axial pre-ionization is important for optimum radiation performance. Furthermore, this gradient provides low EUV radiation reabsorption by the cold gas at the anode side.

The pressure gradient creates a linear mass gradient of the gas along the capillary length. The compression time of the discharge plasma decreases as the linear mass decreases, $t_c \sim \sqrt{m}\frac{cR_0}{I}$, and the plasma near the anode therefore compresses faster than that near the cathode. Such a difference in the compression dynamics effectively causes faster increase of the magnetic field pressure near the anode and produces an axial compression wave along the capillary axis from the anode to the cathode. This effect is demonstrated in the analytical solution for the axially inhomogeneous capillary discharge in the appendix, under the condition that the length of the capillary is much larger than its radius, $l \gg R_0$. It is shown that an axial velocity of the plasma is established as

$$v_z(r,\ z,\ t) = \frac{2r^2}{R}\int_0^t \frac{I^2}{mc^2}\frac{\partial R/\partial z}{R}\,\mathrm{d}t', \tag{22}$$

where the linear mass of plasma $m(z)$ is defined by the initial axial density distribution $\rho_0(z)$, as $m(z) = \pi R_0^2\rho_0(z)$. As a result, the radius of the plasma during compression, R, depends on the time and axial coordinate z (see also the appendix). This solution shows that the plasma flows along the Z-axis from the lower density region to the higher density region and thus the plasma is compressed three dimensionally, unlike the 2D compression in the homogeneous cylindrical case. Formula (22) allows the density distribution $\rho_0(z)$ and capillary profile $(R)_0(z)$ to be optimized for more efficient radiation production.

3.2. Hollow cathode triggered capillary discharge simulations

A set of simulations was performed for fast capillary discharges in a geometry close to the experimental micro plasma pulse (MPP) discharge device established in EPPRA [37, 38]. The MPP radiation source is unique among the DPP sources in operating at a stored electrical energy $<$ 1 J. It relies on very low inductance discharge geometry to allow current of several kiloampere to be delivered to a pre-ionized discharge channel in several nanoseconds, despite the small energy used.

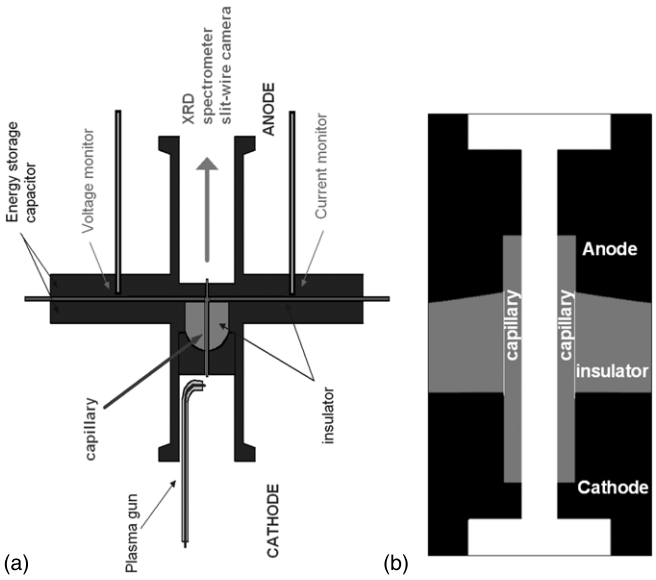

Figure 8. (*a*) Geometry of the EPPRA MPP capillary discharge and (*b*) zoomed view of the capillary region adopted for simulation.

The structure is shown schematically in figure 8(*a*). Various capillary diameters, from 0.8 to 3.2 mm, and lengths 6–12 mm, with various gas and gas compositions, including pure Ar, Kr, Xe or their admixtures with He, at a range of pressures from 1 mTorr to 1 Torr, were examined. These simulations were carried out under different driving parameters, including different cell capacities, cell voltages and different types of generator circuits. Many of these simulation results have been reported at the various EUVL meetings organized by SEMATECH.

To simulate a hollow cathode triggered gas-filled capillary discharge a two-stage approach was applied. In the first, pre-ionization stage, the flow of electrons and ionization processes in their collisions with motionless atoms and ions in the self-consistent electromagnetic field is calculated. Ionization degree distributions and quantity of fast electrons obtained at different time moments are used as initial data for the second stage. In the second, MHD stage, a quasi-neutral plasma dynamics in the self-consistent electromagnetic field and plasma emission is calculated.

3.2.1. Pre-ionization processes. The geometry of the MPP capillary shown in figure 8(*b*) was simulated. An alumina capillary with internal diameter 1.6 mm and length 12 mm is placed between the electrodes. The capillary is filled with argon with an initial pressure 1 Torr. The local energy store is a 0.8 nF capacitor initially charged to 13 kV.

The electric field applied between anode and cathode is distributed in insulators and capillary volume in accordance with Poisson's equation.. Due to the high dielectric constant of alumina $\varepsilon \approx 8.5$ in nanosecond time range the electric field force-lines refract at the capillary internal surface to be concentrated to the capillary axis. The electric field penetrates into the holes in the anode and cathode, which drops exponentially fast with the distance from the holes into the hole volumes of the electrodes.

The electric field accelerates free electrons that are present in a gas. Electrons in the main volume of the capillary are accelerated much too fast to ionize significantly the low-density gas as the ionization cross-section shown in the figure 7 falls very quickly with electron energy. But electrons in the hole volume of the cathode are in the weak electric field and ionize the gas very effectively. The conductive plasma generated pushes out the electric field. In the plasma–gas transition layer the effective ionization process continues leading to the ionization wave propagation [25]. The ionization dynamics obtained is shown in figure 9.

During almost 2 ns an electron beam of several kiloelectron volt energy, initiated near the cathode, passes mainly along the axis of the capillary. The beam is tight, about 70 μm in diameter, due to the action of the combination of the self-magnetic field and the radial component of the external electric field refracted at the gas–dielectric boundary due to the high dielectric constant of the capillary material. The beam and mainly secondary electrons produce ionization in time. At the same time electrons are exposed to the electrostatic turbulence and the dynamics is rather complicated. Near the cathode, the electrons have lower energy and ionize more effectively, while near the anode, where all electrons come together, the ionization also rises more quickly. Due to the increased plasma conductivity, the electric field becomes localized between these clouds of plasma, and ionization waves are observed to move, respectively from the anode and the cathode. From the cathode the wave propagates much faster as the electron energy is close to the optimum of the ionization efficiency (see figure 7). The waves meet each other after 3 ns. At 4 ns the conductive channel occupies half of the diameter of the capillary, but the high density region is localized on-axis. This pre-ionized channel is similar to the initial condition chosen for simulation of the main discharge.

3.2.2. Discharge dynamics Discharge dynamics is examined in the RMHD approach, where the initial conditions with pre-ionized channel are taken from corresponding preliminary electron-hydrodynamic calculations. The capillary is filled with argon with an initial pressure gradient from anode to cathode (35–420 mTorr). The local energy store is 300 mJ. The operating gas is pre-ionized due to the hollow cathode effect and generated electron beam in a tight axial channel. A presence of ~0.1% of fast electrons is taken into account in ionization rate. This portion of fast electrons is chosen from the electron-hydrodynamic calculation and it also coincides with the measured value of the fast electron current [39].

A peak current of 5 kA is obtained with an oscillation half period of 19 ns. The discharge dynamics is presented in figure 10, showing the mass density distribution at different times. Due to the high radiation-cooling rate of the heavy ion plasma, the plasma temperature is relatively low, so that the thermal pressure is less than the magnetic one and the plasma conductivity is low enough to permit penetration of the magnetic field into the plasma column. The capillary discharge plasma compresses volumetrically. Due to the initial gas density gradient along the capillary the lower density plasma is compressed faster and the cumulation in the low-density

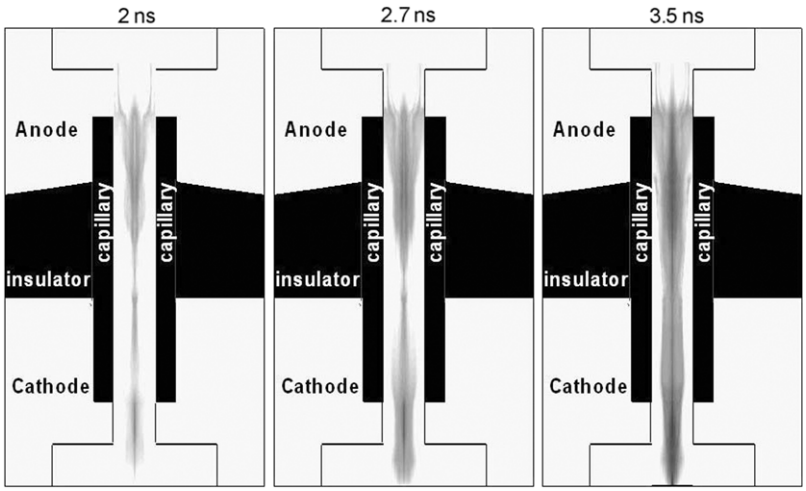

Figure 9. Pre-ionization dynamics of a capillary discharge with iso-contours of ion density n_i shown at different time moments.

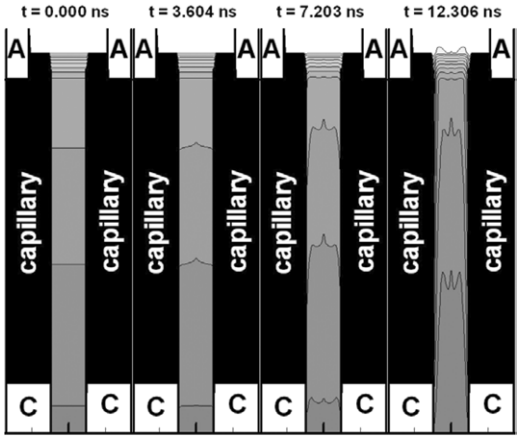

Figure 10. Capillary discharge dynamics in argon with a pressure gradient filled capillary; iso-density contours shown at different time moments.

region generates a compression wave [29] in the direction of the density gradient. The axial wave together with radial magnetic pressure produces a 3D plasma compression. The EUV emission peak is at 7.2 ns. It is produced mainly by relatively dense plasma formed in the initially low-density region near the anode. At the brightest point, the plasma density reaches 5×10^{-7} g cm^{-3} and an electron temperature of $T_e = 18$ eV. The average ionization degree is $Z = 8.8$. This is higher than it corresponds to $T_e = 18$ eV equilibrium value (without fast electrons), which is 7.3. The associated EUV emission in the 13.5 nm 2% bandwidth is 30 μJ/shot, which corresponds to experimental measurements and 5 times higher than the value calculated without fast electrons.

To study the influence of the pre-ionization channel size on the EUV emission yield from the MPP discharge, simulations with different pre-ionization conditions were carried out for a Kr : He gas mixture with Z^*. The results are represented in figure 11(a), which shows the radiation pulse recalculated with transmission function of a Zr filter in two cases; tight on-axis pre-ionization and broad volume pre-ionization. A large first radiation peak is observed for the tight pre-ionization case. In figure 11(b), a series of experimental measurements with a fast

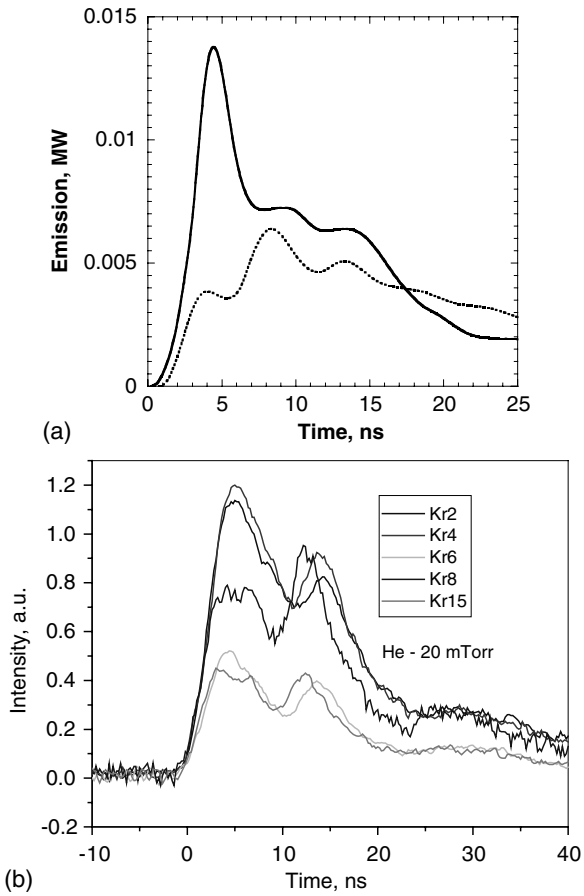

Figure 11. (a) Influence of the pre-ionization channel on EUV emission in the MPP capillary discharge with Kr : He admixture for axial (solid line) and broad (dashed line) pre-ionization obtained in simulations, and (b) experimental measurements behind a Zr filter with different percentage contents of Kr in 20 mTorr of He.

diode behind Zr filter is shown. The measurements were made in discharges with a fixed He pressure of 20 mTorr, measured at the anode side, but with different percentages of Kr admixture. Experimentally, it was shown that a high percentage of Kr leads to a large pre-ionization channel. Qualitative agreement with the simulation results can be seen in the emission.

Simulations with a xenon filled capillary discharge show that EUV emission in the 2% spectral band around 13.5 nm spectral wavelength (the corresponding transition is 5p–4d of XeXI ion) in the optimum may be 5–7 times higher than that from argon [37] with the help of extra ionization of xenon by fast electrons.

4. Summary

To adequately model the multicharged ion plasma in EUV radiation sources, a sufficiently complex physical model has to be developed to take into account the plasma dynamics under the influence of an electromagnetic field, as well as the self-consistent ionization and radiation phenomena. The radiation transport and the ionization kinetics should be able to treat non-equilibrium, non-stationary plasmas under conditions of partial radiation reabsorption. These requirements and the underlying physics description have been briefly discussed in this paper. The solution implemented, in the 2D radiation-MHD code Z^*, satisfies a majority of these requirements. It calculates atomic and ionization properties, EOS, kinetic and transport coefficients, rates of ionization and excitation, and detailed spectral properties of complex ion compound plasma (such as Ar, Xe, Sn) in the non-equilibrium regime. It models plasma dynamics in sophisticated geometries, self-consistently with the radiation transfer in an electromagnetic field.

The RMHD code Z^* allows one to

- carry out complete simulations of plasma radiation sources in geometry and conditions close to the actual experimental set-up,
- evaluate the functionality and suitability of different plasma systems for the purposes of plasma radiation sources,
- define the optimal plasma as well as device parameters for high radiation emission.

In the practical examples given, we have shown how Z^* can be applied to

- obtain a time evolution and dimensions of an EUV radiation emitter,
- study pre-ionization and 3D plasma compression in a gradient capillary discharge,
- evaluate the effect of extra plasma ionization by fast electrons and augmentation of EUV emission from a hollow cathode triggered capillary discharge,
- generally optimize geometries and plasma conditions for better EUV radiation yield.

Appendix

The dynamics of a solid-filled, current carrying cylindrical plasma channel, being set in motion by the self-azimuthal magnetic field B, under the condition of negligible thermal pressure with respect to the magnetic one $\frac{p}{B^2/8\pi} \ll 1$, is described by simplified MHD equations following from equation (1), neglecting thermal pressure, displacement current and electron drift velocity:

$$\rho\left(\frac{\partial v_r}{\partial t} + v_r\frac{\partial v_r}{\partial r} + v_z\frac{\partial v_r}{\partial z}\right) = -\frac{1}{c}j_z B \tag{A1.1}$$

$$\rho\left(\frac{\partial v_z}{\partial t} + v_r\frac{\partial v_z}{\partial r} + v_z\frac{\partial v_z}{\partial z}\right) = \frac{1}{c}j_r B \tag{A1.2}$$

$$\frac{\partial \rho}{\partial t} + \frac{1}{r}\frac{\partial}{\partial r}(r\rho v_r) + \rho\frac{\partial v_z}{\partial z} + v_z\frac{\partial \rho}{\partial z} = 0 \tag{A1.3}$$

$$\frac{\partial B}{\partial t} + \frac{\partial}{\partial r}(v_r B) + \frac{\partial}{\partial z}(v_z B) = \frac{\partial}{\partial r}\left(\frac{D}{r}\frac{\partial}{\partial r}(rB)\right) + \frac{\partial}{\partial z}D\frac{\partial B}{\partial z} \tag{A1.4}$$

$$\frac{4\pi}{c}j_r = -\frac{\partial B}{\partial z}; \quad \frac{4\pi}{c}j_z = \frac{1}{r}\frac{\partial}{\partial r}(rB), \tag{A1.5}$$

where $D = \frac{c^2}{4\pi\sigma_\perp}$, $\sigma_\perp$ is the plasma conductivity transverse to the magnetic field.

Let us consider first only weak variations along the channel length, i.e. $\partial/\partial z \ll \partial/\partial r$. In a zeroth approximation, when the variables are independent of the Z coordinate i.e. $\partial/\partial z = 0$, we have $j_r = 0$ and $v_z = 0$.

At sufficiently fast diffusion, $t \gg R^2/D$ (R is the plasma column radius), the density of the longitudinal current is constant inside the plasma, i.e. at $r < R$:

$$j_z = \frac{I}{\pi R^2}, \qquad B = \frac{2I}{c}\frac{r}{R^2}, \tag{A1.6}$$

where $I(t)$ is the current. The column radius $R(t)$ decreases in time due to plasma compression under Ampere force. From equation (A1.4) and (A1.3) it follows that

$$v_r = r\frac{\dot{R}}{R}, \tag{A1.7}$$

$$\rho = \rho_0\frac{R_0^2}{R^2}, \tag{A1.8}$$

where we denote the time derivative $\partial/\partial t$ by a dot, R_0 is the initial plasma radius. As follows from (A1.1) and (A1.6, 7), the plasma radius is described by the equation:

$$\ddot{R} = -\frac{2}{mc^2}\frac{I^2}{R}, \tag{A1.9}$$

where the plasma mass per unit length is $m = \pi R_0^2\rho_0 = \pi\rho R^2$. This type of equation is often encountered in the theory of magnetically driven liners and Z-pinches. We introduce dimensionless variables: $\xi = \frac{R_0}{R}$ and $\tau = \frac{t}{t_0}$, where $t_0 = \sqrt{m}\frac{cR_0}{I_0}$ and I_0 is the current amplitude. For a constant current $I(t) = I_0$ the solution is

$$\tau(\xi) = \frac{\sqrt{\pi}}{2}\mathrm{Erf}(\sqrt{\ln\xi}), \tag{A1.10}$$

where $\mathrm{Erf}(x)$ is the error function. The formal compression time, when $R \to 0$, i.e. $\xi \to \infty$ and $\tau(\infty) = \sqrt{\pi}/2 \approx 0.89$, is $t_c \approx t_0$.

If the plasma density or the radius of the plasma channel depends on the Z-coordinate, i.e. $\rho_0(z)$ or $R_0(z)$, in first order

approximation for non-homogeneity the radial component of current density is not zero:

$$j_r = \frac{Ir}{\pi R^3}\frac{\partial R}{\partial z}. \qquad \text{(A1.11)}$$

It is important to note here that $R(z,t)$, $\dot{R}$ and $\partial R/\partial z$ are functions of time t (equation (A1.9)) and coordinate z (depending only on $\rho_0(z)$, as $m = \pi R_0^2\rho_0$). Replacing equation (A1.2) by (A1.6) and (A1.11) in the first order approximation the axial motion is described by the following equation:

$$\dot{u} = \frac{2I^2}{mc^2}\frac{\partial R/\partial z}{R}, \qquad \text{(A1.12)}$$

where $v_z = u(z,t)\frac{r^2}{R^2}$. A solution satisfying the initial condition $u(t=0)=0$ is:

$$v_z(r,z,t) = \frac{2r^2}{R^2}\int_0^t \frac{I^2}{mc^2}\frac{\partial R/\partial z}{R}dt' \qquad \text{(A1.13)}$$

In particular, for the case when a current $I(t) = I_0$ and the initial plasma column radius R_0 are constant, the integral in (A1.13) may be taken with the help of the relation (A1.9) and solution (A1.10). For the axial velocity we obtain a solution:

$$v_z(r,\ z,\ t) = \frac{r^2}{2t_0\sqrt{\ln\left(\frac{R_0}{R}\right)}}\frac{R_0}{R}$$
$$\times\left[\ln\left(\frac{R_0}{R}\right)\left(1+\frac{t}{t_0}\right) - \frac{t}{2t_0}\right]\frac{\partial \ln\rho_0}{\partial z}. \qquad \text{(A1.14)}$$

This solution demonstrates that equations (A1.9), (A1.12) and (A1.13) describe plasma flow along the axis and the plasma column compression. The plasma flows along the Z-axis from lower density to higher density and is compressed by radius. So, the plasma is compressed three dimensionally, unlike 2D compression in the homogeneous cylindrical case.

References

[1] 2003 *International Technology Road Map for Semiconductors (ITRS)* 2003 edition (www.sematech.org)

[2] O'Sullivan G and Carroll P K 1981 4d–4f emission resonances in laser-produced plasmas *J. Opt. Soc. Am.* **71** 227

[3] Zakharov S V, Novikov V G and Choi P 2005 Z*-code for DPP and LPP source modelling *EUV Sources for Lithography* ed V Bakshi (Bellingham, WA: SPIE Optical Engineering Press) p 223

[4] Zakharov S V *et al* 1994 *ZETA Code: Physical Models and Numerical Algorithms* (Moscow: KIAM)

[5] Benattar R *et al* 1999 Influence of magnetohydrodynamic Rayleigh–Taylor instability on radiation of imploded heavy ion plasmas *Phys. Plasmas* **6** 175

[6] Zakharov S V, Choi P, Krukovskiy A, Zhang Q, Novikov V G and Zakharov V S 2005 *6th Int. Conf. on Dense Z-pinches (Oxford, UK)* ed J Chittenden *AIP Conf. Proc.* **808** 275

[7] Zakharov S V, Choi P, Novikov V G, Zakharov V S and Krukovskiy A Y 2006 *Proceeding website. EUV Source Workshop (Barcelona, Spain, 19 October 2006)*

[8] Braginskii S I 1965 *Reviews of Plasma Physics* (New York: Consultants Bureau) **1** 205

[9] Nikiforov A F, Novikov V G and Uvarov V B 2005 *Quantum-Statistic Models of Hot Dense Matter and Methods for Computation of Opacity and Equation of State* (Basle: Birkhauser)

[10] Rozsnyai B F 1997 Collisional-radiative average-atom model for hot plasmas *Phys. Rev.* E **55** 7507

[11] Novikov V G and Zakharov S V 2003 Modeling of non-equilibrium radiating tungsten liners *J. Quant. Spectrosc. Radiat. Transfer* **81** 339–54

[12] Novikov V G, Zakharov V S, Nikiforov A F, Zakharov S V and Choi P 2004 Ionization and excitation rate calculations in nonequilibrium plasma of EUV source *Source Workshop (Santa Clara, 22 February 2004)*

[13] Post D E *et al* 1977 Steady-state radiative cooling rates for low density high temperature plasmas *At. Data Nucl. Data Tables* **20** 397–439

[14] Busquet M 1993 Radiation dependent ionization model for laser-created plasmas *Phys. Fluids* B **5** 4191–206

[15] Novikov V G and Solomyannaya A D 1998 Spectral characteristics of plasma consistent with radiation *High Temp.* **36** 858–64 (in Russian)

[16] Sobelman I I, Vainshtein L A and Yukov E A 1981 *Excitation of Atoms and Broadening of Spectral Lines* (Berlin: Springer)

[17] Lotz W 1968 *Z. Phys.* **216** 241

[18] Zakharov V S and Novikov V G 2005 *6th Int. Conf. on Dense Z-Pinches (Oxford, UK) AIP Conf. Proc.* **808** 323

[19] Mihalas D 1978 *Stella Atmospheres* 2nd edn (San Francisco: Freeman)

[20] Zakharov V S, Novikov V G and Zakharov S V 2005 Impact ionization and excitation of multicharged ions in DPP and LPP *Proc. Website 4th EUVL Symp. (San Diego, CA, November 2005)*

[21] Zakharov V S and Novikov V G 2006 *18th ESCAMPIG (Lecce, Italy, 12–16 July 2006)*

[22] de Heer F J, Jansen R H J and Van der Kaay W 1979 *J. Phys. B: At. Mol. Phys.* **12** 979

[23] Gu M F Flexible atomic code (http://kipac-tree.stanford.edu/fac/)

[24] Choi P and Favre M 1998 Fast pulsed hollow cathode capillary discharge device *Rev. Sci. Instrum.* **69** 3118–22

[25] Mond M, Rutkevich I, Kaufman Y, Choi P and Favre M 2000 Ionization waves in electro-beam-assisted, shielded capillary discharge *Phys. Rev.* E **62** 5603

[26] Leontovich M A and Osovets S M 1956 About mechanism of current compression at fast and powerfull gas discharge *At. Energy* **3** 81

[27] D'yachenko V F and Imshennik V S 1974 Two-dimensional magnetohydrodynamic model of Z-pinch plasma focus *Rev. Plasma Phys.* **8** 164 (in Russian) (Moscow: Atomizdat)

[28] Choi P and Dumitrescu-Zoita C 1997 On the radiative collapse phenomenon *4th Int. Conf.* on *Dense Z-Pinches (Vancouver, Canada 1997) AIP Conf. Proc.* **409** 51

[29] Zakharov S V and Choi P 2001 The radiation magnetohydrodynamics of a nanosecond capillary discharge *Proc. IEEE Conf. Rec. Pulsed Power Plasma Science (Las Vegas, NV, 2001)* 73

[30] Grigor'ev S F and Zakharov S V 1987 Magnetohydrodynamics of an intensely emitting liner plasma *Sov. Tech. Phys. Lett.* **13** 254

[31] Jushkina L, Chuvatin A, Zakharov S V, Ellwi S and Kunze H-J 2002 EUV emission from Kr and Xe capillary discharge plasmas *J. Phys. D: Appl. Phys.* **35** 219–27

[32] Zakharov S V, Choi P, Novikov V G, Zakharov V S and Krukovskiy A Y 2006 Update on EUV source modeling benchmarking *EUV Source Workshop (Barcelona, Spain, 19 October 2006)*

[33] Zakharov S V, Choi P, Krukovskiy À, Zhang Q, Novikov V G, Zakharov V S and Solomyannaya A D 2004 Modelling of the non-equilibrium plasmas of EUV sources *3rd Int. EUVL Symp. (Miyazaki, Japan, 1–4 November 2004)* 3-07So16

[34] Zakharov S V 2006 Modeling with the code Z* of EUV emission and fast particles generation in DPP and LPP sources *EUV Source Workshop (Baltimore, MD, 6 May 2006)*

[35] de Bruijn R, Koshelev K, Zakharov S and Bijkerk F 2005 Enhancement of laser plasma extreme ultraviolet emission by shockwave-laser interaction *Phys. Plasmas* 12 04,2701

[36] Zakharov S V, Choi P, Krukovskiy A, Zhang Q, Novikov V G, Zakharov V S and Solomyannaya A D 2005 A black-box modeling engine for optimization modeling of EUV plasma sources *Proc. Website 4th EUVL Symp. (San Diego, CA, November 2005)*

[37] Choi P, Zakharov S, Aliaga-Rossel R, An Y, Dumitrescu C, Leblanc C, Sarroukh O and Zakharov V 2006 *Proc. Website. EUVL Symp.(Barcelona, Spain, 15–18 October 2006)*

[38] Choi P, Aliaga-Rossel R, Bouamra K, An Y, Zakharov S V and Zakharov V S 2005 *Proc. Website. 4th EUVL Symp. (San Diego, CA, November 2005)*

[39] Favre M, Choi P, Chuaqui H, Mitchell I, Wyndham E and Leñero A M 2003 Experimental investigation of ionization growth in the pre-breakdown phase of fast pulsed capillary discharges *Plasma Sources Sci. Technol.* **12** 78–84

[40] Krisch I, Choi P, Larour J, Favre M, Rous J and Leblanc C 2000 A compact ultrafast capillary discharge for EUV projection lithography *Contrib. Plasma Phys.* **40** 135